Int. J. Heat Mass Transfer. Vol. 36, No. 9, pp. 2429–2440, 1993
Printed in Great Britain

0017-9310/93 $6.00+0.00

Developing laminar flow and heat transfer in a square duct with one-walled injection and suction

G. J. HWANG and Y. C. CHENG
Department of Power Mechanical Engineering, National Tsing Hua University, Hsinchu, Taiwan 300, R.O.C.

and

M. L. NG
Energy and Resources Laboratories, Industrial Technology Research Institute, Hsinchu, Taiwan 310, R.O.C.

(*Received* 18 *June* 1992 *and in final form* 7 *October* 1992)

Abstract—A numerical study was made to investigate the forced laminar convection in the entrance region of a square duct with one wall subjected to uniform mass transpiration and constant heat flux. Using the concept of pressure deviation and the vorticity–velocity method, the three-dimensional Navier–Stokes equations and the governing energy equation were solved simultaneously. Results show that flow reversal occurs in the flow with strong suction. Typical velocity, pressure and temperature distributions along the flow direction are reported. Both local friction factors and Nusselt numbers in the developing and fully developed regions are examined. The Prandtl number effect is also discussed in the present numerical analysis.

INTRODUCTION

DUE TO applications in nuclear reactors, turbine engines, combustion chambers, solar collectors and electrochemical systems, the fluid flow and heat transfer in channels with fluid transfer at the boundary have received a great deal of attention in the past. Reviews of this subject can be found in Raithby and Knudsen [1] and Rhee and Edwards [2], as well as Soong and Hwang [3]. Most investigations deal mainly with uniform and symmetric transpiration as well as heating for porous tubes or parallel plates. Only a few studies [2, 4–8] report the results of semi-porous parallel plates.

Previously, two-dimensional models were usually used to treat this problem in a three-dimensional duct flow with fluid transfer on boundaries. From an engineering point of view, only ducts with very small height/width aspect ratios can be treated as parallel plates. However, many applications are known to have a considerably high aspect ratio, as can be seen in the reactant gas flows in fuel cells [9]. Figure 1 is a schematic diagram showing flows of gases in fuel cells. Both cathode and anode gases are channeled to the electrodes by many small parallel square ducts. Through the porous electrodes of fuel cells, reactants and heat can be exchanged to maintain a steady operating condition. Thus the flow of reactant gases in a fuel cell can be treated as the flow in one-porous-wall square ducts at constant heat flux boundary condition [10].

In this study, a three-dimensional model is used to describe the flow and temperature fields in a square duct with one wall subjected to uniform fluid injection or suction and heat transfer with constant heat flux. Both flow and heat transfer characteristics in developing laminar flow are analyzed numerically.

THEORETICAL ANALYSIS

Consider a steady laminar flow of an incompressible fluid with constant thermophysical properties in a square duct, as shown in Fig. 1. Both axial velocity and temperature distributions of the fluid are uniform before entering the square duct. The lower wall of the duct is porous and subjected to constant heat flux, while the other three walls are impermeable and adiabatic. Fluid flow with uniform injection or suction is imposed at the porous wall. This injection or suction fluid is the same as that of the duct flow and has the same temperature of the heated porous wall. External forces, compression work and viscous dissipation are neglected.

By using the concept of pressure deviation, the pressure term can be written as

$$P(X, Y, Z) = P_0 + \bar{P}(X) + P'(X, Y, Z) \qquad (1)$$

where P_0 is the uniform inlet pressure, $\bar{P}(X)$ the additional pressure averaged over the cross section at axial location X, and $P'(X, Y, Z)$ the pressure deviation in the transverse direction. Referring to the

NOMENCLATURE

A cross-sectional area
D side length of square duct
D_h hydraulic diameter, $4A/S$
f friction factor, $2\bar{\tau}_w/(\rho\bar{U}^2)$
h heat transfer coefficient
k thermal conductivity
M, N number of grids in y- and z-directions, respectively
Nu local Nusselt number, hD_h/k
P, p pressure and dimensionless pressure
P', p' pressure deviation and dimensionless pressure deviation induced by fluid injection or suction
$\bar{P}, \bar{p}$ pressure and dimensionless pressure averaged over a cross section
Re local Reynolds number, $\bar{U}D_h/\nu$
Re_w wall Reynolds number, V_wD_h/ν
S perimeter
T temperature
u, v, w dimensionless velocity components in the x-, y- and z-directions, respectively
U, V, W velocity components in the X-, Y- and Z-directions, respectively
x, y, z dimensionless rectangular coordinates
X, Y, Z rectangular coordinates.

Greek symbols
α thermal diffusivity
ε criterion of convergence
θ dimensionless temperature
μ viscosity
ν kinematic viscosity
ξ vorticity defined by equation (9)
ρ density
τ shear stress.

Subscripts
b bulk fluid condition
fd values in fully developed region
j, k nodal point of a cross section
w wall condition
0 inlet condition
1, 2 values derived by averaged local gradient and overall balance, respectively.

Superscripts
— average value
n step number in the axial direction
$+$ definition for $x^+ = x/Pr$.

coordinate system in Fig. 1, the following dimensionless variables and parameters can be introduced:

$$x = X/(D_h\,Re_0), \quad y = Y/D_h, \quad z = Z/D_h$$
$$u = U/U_0, \quad v = VD_h/\nu, \quad w = WD_h/\nu$$
$$\bar{p} = \bar{P}/(\rho U_0^2), \quad p' = P'D_h^2/(\rho\nu^2)$$
$$\theta = (T-T_0)/(qD_h/k), \quad Re_0 = U_0D_h/\nu$$
$$Re_w = V_wD_h/\nu, \quad Pr = \nu/\alpha. \tag{2}$$

At high Reynolds number $Re_0^2 \gg 1$, the axial diffusion terms in the three momentum equations and the axial conduction term in the energy equation can be

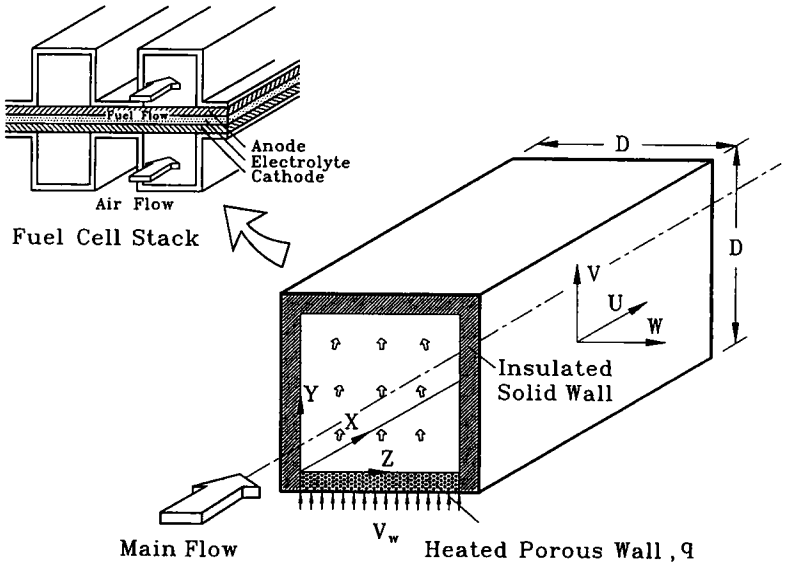

FIG. 1. Schematic diagram for a fuel cell and the coordinate system.

neglected. Hence the following dimensionless equations are obtained:

$$\frac{\partial u}{\partial x}+\frac{\partial v}{\partial y}+\frac{\partial w}{\partial z}=0 \tag{3}$$

$$u\frac{\partial u}{\partial x}+v\frac{\partial u}{\partial y}+w\frac{\partial u}{\partial z}=-\frac{\mathrm{d}\bar{p}}{\mathrm{d}x}+\frac{\partial^2 u}{\partial y^2}+\frac{\partial^2 u}{\partial z^2} \tag{4}$$

$$u\frac{\partial v}{\partial x}+v\frac{\partial v}{\partial y}+w\frac{\partial v}{\partial z}=-\frac{\partial p'}{\partial y}+\frac{\partial^2 v}{\partial y^2}+\frac{\partial^2 v}{\partial z^2} \tag{5}$$

$$u\frac{\partial w}{\partial x}+v\frac{\partial w}{\partial y}+w\frac{\partial w}{\partial z}=-\frac{\partial p'}{\partial z}+\frac{\partial^2 w}{\partial y^2}+\frac{\partial^2 w}{\partial z^2} \tag{6}$$

$$u\frac{\partial \theta}{\partial x}+v\frac{\partial \theta}{\partial y}+w\frac{\partial \theta}{\partial z}=\frac{1}{Pr}\left(\frac{\partial^2\theta}{\partial y^2}+\frac{\partial^2\theta}{\partial z^2}\right). \tag{7}$$

By going through an order of magnitude analysis [11], the dimensionless pressure gradient, $\mathrm{d}\bar{p}/\mathrm{d}x$, can be seen as a function of x only. The term $-(1/\rho)(\partial P'/\partial X)$ in equation (4) is then eliminated under high entrance Reynolds number conditions. The initial and boundary conditions can be written as:

$u-1=v=w=\theta=0$ at entrance, $x=0$

$u=v-Re_w=w=\partial\theta/\partial y+1=0$ at porous wall, $y=0$

$u=v=w=\partial\theta/\partial y=0$ at impermeable wall, $y=1$

$u=v=w=\partial\theta/\partial z=0$ at impermeable walls, $z=0,1$ (8)

where the value of Re_w is positive for injection flows, negative for suction flows and zero for impermeable flows. Thus the solution of these equations depends on two independent parameters: the wall Reynolds number, Re_w, for the porous wall and the Prandtl number, Pr, in an energy equation.

A vorticity–velocity method has been successfully developed [11, 12] and will be used for the present study. A vorticity function in the axial direction is defined as:

$$\xi=\frac{\partial w}{\partial y}-\frac{\partial y}{\partial z}. \tag{9}$$

By differentiating equation (9) and combining with the continuity equation (3), the following equation can be derived:

$$\frac{\partial^2 v}{\partial y^2}+\frac{\partial^2 v}{\partial z^2}=-\frac{\partial \xi}{\partial z}-\frac{\partial^2 u}{\partial y\,\partial x} \tag{10}$$

$$\frac{\partial^2 w}{\partial y^2}+\frac{\partial^2 w}{\partial z^2}=\frac{\partial \xi}{\partial y}-\frac{\partial^2 u}{\partial z\,\partial x}. \tag{11}$$

Then the governing equations (3), (5) and (6) can be put into the final vorticity–velocity form. The pressure terms in equations (5) and (6) are eliminated by cross differentiations, and a single equation for the axial vorticity can now be obtained:

$$u\frac{\partial \xi}{\partial x}+v\frac{\partial \xi}{\partial y}+w\frac{\partial \xi}{\partial z}+\xi\frac{\partial v}{\partial y}+\xi\frac{\partial w}{\partial z}+\frac{\partial u}{\partial y}\frac{\partial w}{\partial x}-\frac{\partial u}{\partial z}\frac{\partial v}{\partial x}=\frac{\partial^2\xi}{\partial y^2}+\frac{\partial^2\xi}{\partial z^2}. \tag{12}$$

Equations (4), (10), (11) and (12) are used for solving u, v, w and ξ, respectively. An additional constraint to determine $\mathrm{d}\bar{p}/\mathrm{d}x$ in equation (4) can be derived from the overall mass balance. This can be expressed as

$$\bar{u}=1+Re_w x \tag{13}$$

where $\bar{u}$ is the averaged axial velocity obtained from the solution of the same equation.

After the velocity and temperature fields along the axial direction in the developing region are obtained, local friction factors can be computed based on the velocity gradients at the walls, as seen in equation (14). Another friction factor can be derived from the overall force balance for a unit axial length in the flow:

$$(f\,Re)_1=\frac{1}{2\bar{u}}\left[\int_0^1\left.\frac{\partial u}{\partial y}\right|_{y=0}\mathrm{d}z-\int_0^1\left.\frac{\partial u}{\partial y}\right|_{y=1}\mathrm{d}z+2\int_0^1\left.\frac{\partial u}{\partial z}\right|_{z=0}\mathrm{d}y\right] \tag{14}$$

$$(f\,Re)_2=\frac{1}{2\bar{u}}\left[\left(-\frac{\mathrm{d}\bar{p}}{\mathrm{d}x}\right)-\frac{\partial\overline{u^2}}{\partial x}\right]. \tag{15}$$

Similarly, local Nusselt numbers can also be calculated from the average temperature difference between the heated wall and the bulk mean fluid as well as from an overall energy balance for a unit axial length:

$$(Nu)_1=\frac{1}{\overline{\theta_w-\theta_b}} \tag{16}$$

$$(Nu)_2=Pr\left[\frac{\bar{u}}{\overline{\theta_w-\theta_b}}\frac{\partial\theta_b}{\partial x}-Re_w\right] \tag{17}$$

where θ_b is the bulk mean temperature defined as

$$\theta_b=\frac{1}{\bar{u}}\int_0^1\int_0^1 u\theta\,\mathrm{d}y\,\mathrm{d}z. \tag{18}$$

METHOD OF SOLUTION

To find a solution mathematically for the unknowns, u, v, w, ξ and θ in equations (4), (7), (10)–(12) satisfying the initial and boundary conditions in equation (8) is beyond contemplation. A numerical finite difference scheme based on the vorticity–velocity method [11] is employed to obtain the simultaneous solutions for each desired axial location at different Re_w and Pr. The step-by-step procedure is:

(1) Assign initial values for the velocity components and temperature difference, $u=v=w=$

$\theta = 0$, and thus $\xi = 0$ at $x = 0$ which is from equation (9).

(2) Using a guessed value for the axial pressure term, $-\mathrm{d}\bar{p}/\mathrm{d}x$, find new values of u and ξ at interior points of the next axial position from equations (4) and (12), respectively, by the Du Fort–Frankel method [13].

(3) Check if the constraint for the average axial velocity $\bar{u}$ in equation (13) is satisfied. If not, adjust the value of the pressure term in equation (4) and repeat steps 2 and 3.

(4) Determine the local friction factor $f\,Re$ along the axial flow direction of the duct from equation (14).

(5) Solve the elliptic-type equations (10) and (11) for v and w by using the alternating direction implicit scheme [14]. During the iteration process, values of vorticity ξ on boundaries are evaluated simultaneously with v and w in the interior region. These boundary vortices on the four walls are evaluated by using the method of Chou and Hwang [11].

(6) Repeat step 5 until the following criteria are satisfied for velocity components v and w:

$$\varepsilon_1 = \Sigma|(v_{j,k}^{(n+1)} - v_{j,k}^{(n)})/v_{j,k}^{(n+1)}|/(M \cdot N) \leqslant 5 \cdot 10^{-4} \tag{19}$$

$$\varepsilon_2 = \Sigma|(w_{j,k}^{(n+1)} - w_{j,k}^{(n)})/w_{j,k}^{(n+1)}|/(M \cdot N) \leqslant 5 \cdot 10^{-4} \tag{20}$$

where M and N are the numbers of divisions in the y- and z-directions.

(7) Obtain new values of θ at the interior points of the next axial location from equation (7) by the Du Fort–Frankel method. Using the boundary conditions in equation (8), compute the temperature at the walls of the duct after the temperature in the interior region is calculated.

(8) Calculate the bulk mean temperature from equation (18), and the local Nusselt number from equation (16).

(9) Repeat steps 2–8 at the next axial position until the desired axial location is reached.

A uniform cross-sectional grid of 41×41 with fixed axial step size 5×10^{-5} was used for the full domain of the square duct. Numerical experiments were carried out to ensure the independence of the results on the mesh and step sizes. These tests have been performed even at strong injection and suction conditions which cause stiff velocity and temperature gradients. Table 1 presents the values of $f\,Re$ and Nu at $Re_w = 20$ and -20 for fluid with $Pr = 0.72$. For the cases of grids 41×41 and 51×51 with step sizes 5.0×10^{-5} and 2.5×10^{-5}, respectively, all of the predicted friction factors, $(f\,Re)_1$, and Nusselt numbers, $(Nu)_1$, change by less than 1% at all axial positions. The results of the calculations using grid numbers 41×41 and 51×51 for $(f\,Re)_1$, $(f\,Re)_2$ and $(Nu)_1$ are close enough for all cases in this study. However, the values of $(Nu)_2$ using grid numbers 41×41 and 51×51 differ greatly at $x = 0.05$ and 0.1 for injection flow $Re_w = 20$. This is understandable from equation (17) in that subtraction of two large values of the order of 10 does not yield an accurate small number around 0.5. Hence, values of $(f\,Re)_1$ and $(Nu)_1$ will be used in the present study for their better accuracy.

Table 1. Numerical experiments for grid and step sizes ($Pr = 0.72$)

		20		−20†	
Re_w					
Grid No. ($M \times N$)		41 × 41‡	51 × 51	41 × 41‡	51 × 51
Step size × 10^4		0.5	0.25	0.5	0.25
$x = 0.001$,	$(f\,Re)_1$	32.00	31.99	37.38	37.56
	$(f\,Re)_2$	33.66	32.93	39.58	38.97
$x = 0.005$,	$(f\,Re)_1$	22.78	22.84	24.87	25.08
	$(f\,Re)_2$	23.07	23.11	25.71	25.73
$x = 0.01$,	$(f\,Re)_1$	21.32	21.39	22.16	22.38
	$(f\,Re)_2$	21.49	21.56	22.91	22.99
$x = 0.05$,	$(f\,Re)_1$	20.67	20.78		
	$(f\,Re)_2$	20.83	21.02		
$x = 0.1$,	$(f\,Re)_1$	20.67	20.82		
	$(f\,Re)_2$	20.82	21.06		
$x = 0.001$,	$(Nu)_1$	7.580	7.666	22.85	23.02
	$(Nu)_2$	7.447	7.644	22.99	23.11
$x = 0.005$,	$(Nu)_1$	2.345	2.339	17.04	16.97
	$(Nu)_2$	2.245	2.378	16.85	16.87
$x = 0.01$,	$(Nu)_1$	1.398	1.390	15.90	15.81
	$(Nu)_2$	1.317	1.426	15.70	15.71
$x = 0.05$,	$(Nu)_1$	0.527	0.523		
	$(Nu)_2$	0.706	1.011		
$x = 0.1$,	$(Nu)_1$	0.410	0.408		
	$(Nu)_2$	0.556	1.053		

† Flow reversal at $x = 0.0294$.

‡ The number of grids and step sizes used through the present study.

As a partial verification of the computational results, the hydrodynamically developing flow was calculated without mass transpiration. These results are compared with Shah and London [15] and Curr *et al.* [16]. As shown in Table 2, the difference in the friction factors are within 1% at all axial locations. Due to the lack of simultaneously developing flow data for square ducts with one heated wall in the open literature, only the fully developed Nusselt number is compared. Table 3 shows that this peripherally averaged Nusselt number agrees within 1.2% to that of Schmidt and Newell [17] for the thermally developed result. These calculations were performed on a minicomputer, VAX 6310. Typical computation time was approximately 30–60 CPU min for the axial distance

Table 2. Comparison of friction factors of impermeable duct flow

x	Refs. [15, 16]	This study
0.001	111.0	111.6
0.005	51.8	51.87
0.01	38.0	38.27
0.05	21.0	21.21
0.1	17.8	17.86

Table 3. Fully developed friction factors and heat transfer results for injection flow

Re_w	$(u/\bar{u})_{max}$	$f\,Re$	Nu ($Pr = 0.72$)
0	2.093 [15]	14.23 [15]	2.712 [17]
0	2.097	14.17	2.681
5	2.020	15.73	1.312
10	1.968	17.49	0.692
20	1.893	20.65	0.297

$x = 0.1$. It is noted that the computation time depends mainly on the length of axial distance and the magnitude of injection or suction velocity through the porous wall.

RESULTS AND DISCUSSION

Detailed results for injection and suction through the porous wall of a square duct are now given separately below. Although the study of friction factors and Nusselt numbers in the entrance region is the major goal here, the velocity and temperature fields of the developing region are important in clarifying the heat transfer mechanism and will be discussed. Results of the axial pressure, porous wall and bulk mean temperature will be presented in detail for understanding the problem. Moreover, the effects of flow reversal and Prandtl number on heat transfer characteristics are also presented.

Axial velocity

In the case of injection flow, the development of axial velocities for different locations along the axial direction is presented in Fig. 2(a) for wall Reynolds number $Re_w = 5$. As can be seen, fluid injection increases the axial velocity components of the flow in the duct and shifts its peak towards the solid wall opposite to the porous wall. Although this shift is not significant near the inlet, the trend is more pronounced as the axial distance increases. In addition, the maximum dimensionless velocity, $(u/\bar{u})_{max}$, reaches a maximum value (2.020 as shown in Table 3 for $Re_w = 5$) at a certain point in the cross-section and the flow can be considered as fully developed subsequently. Figure 2(a) also shows that the shape of whole axial velocity profile is close to a skew-type paraboloid in the fully developed region. The case for suction flow with $Re_w = -5$ is presented in Fig. 2(b) for comparison. Similar to the injection flow, the boundary layer of the suction flow is too thin to affect the main flow near the inlet ($x = 0.001$), and hence the axial velocity profile is almost flat across the cross section. Moving away from the inlet, the effect of suction becomes more apparent as shown by the velocity components shrinking along the axial distance. Figure 2(b) shows that the shift of the velocity profile appears also in the suction flow with its peak moving toward the porous wall due to the outward suction force.

The effect of Re_w on the axial velocity profile is

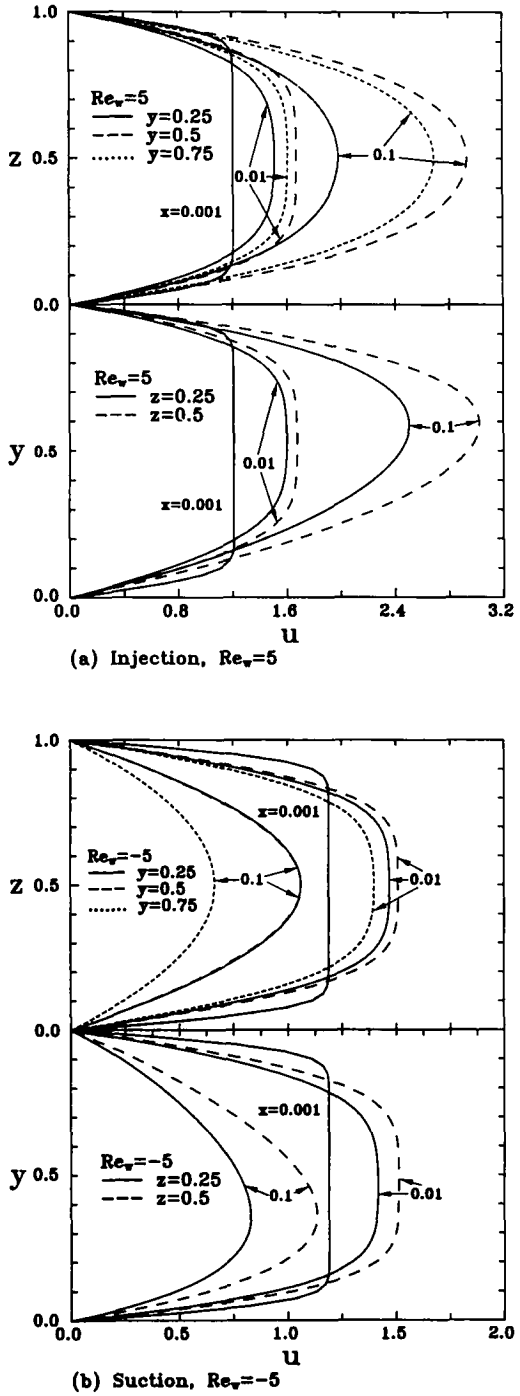

FIG. 2. Axial velocity distribution in cross section at different axial distances: (a) injection, $Re_w = 5$; (b) suction, $Re_w = -5$.

illustrated in Fig. 3. In general, the boundary layer thickness is larger for the injection flow than suction flow at the same axial position for the same absolute value of wall Reynolds number in the entrance region. It is also evident that the shift of axial velocity profile begins at the entrance and is continuously moving toward a fixed position which is dependant on the wall Reynolds number. This shift is more pronounced

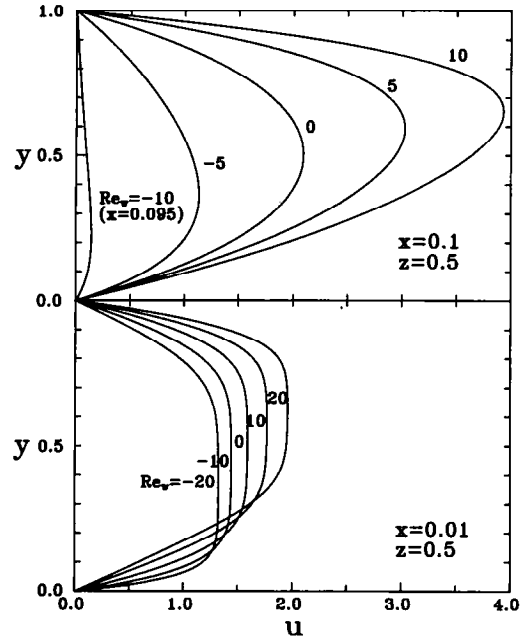

FIG. 3. Wall Reynolds number effects on axial velocity distributions at different axial distances.

for both injection and suction flows at more extreme wall Reynolds numbers.

Flow reversal

As noted by Quaile and Levy [18], the laminar tube flow with fluid extraction can be changed to turbulence at a sufficiently negative wall Reynolds number. For the developing laminar flow between semiporous parallel plates with nonuniform suction, flow reversal in the velocity field has been reported by Sorour *et al.* [8]. In the present study, flow reversal can also be found for suction flows in a one-porous-wall square duct. Locations of complete mass suction and flow reversal are plotted over a range of wall Reynolds numbers in Fig. 4. It is noted that the flow reversal occurs earlier at more negative Re_w due to the stronger outward suction force.

When the fluid is extracted from the porous wall of a square duct, its mass flow in the local cross section diminishes along the duct and vanishes at the point of complete mass extraction. But in a large suction flow, the rate of replenishment by the fluid in the cross-section filling the vacancies caused by extraction may not be sufficient, and thus flow reversal is created at that specific axial position. According to the calculated results of axial velocity distribution for suction flow, the regions of the minimum flow velocity in the cross section are at the upper left and right corners of the duct where negative axial velocities first appear. The critical wall Reynolds number is found to be -11.5 for flow reversal in this square duct. The flow reversal occurs because axial mass but no axial momentum is withdrawn ($u_w = 0$). Hence the axial momentum decreases and must be balanced by a pressure rise. This adverse pressure gradient reverses the flow where its velocity is already small—near the upper corners.

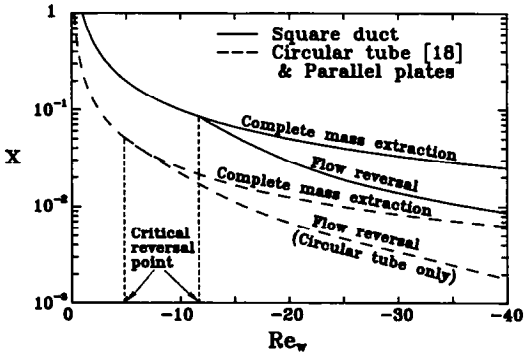

FIG. 4. Complete mass extraction and flow reversal under different suction conditions.

Transverse velocity

It is obvious that the hydrodynamics of fluid flow can be further understood if the transverse velocity in the cross section is analyzed. The information about flow field development is provided via vector plots of the secondary flow along the channel for both cases of injection and suction, as depicted in Figs. 5(a) and (b). In the inlet region ($x = 0.001$), flow resistance is larger near the channel walls, and hence fluid moves toward the so-called 'hydrodynamic center'. However, the position of this hydrodynamic center is skewed upward from the geometric center for injection flow and downward for suction flow until close to the fully developed region ($x = 0.1$), the hydrodynamic center disappears. Thus, the direction of transverse velocity in the cross section is moved upward in the case of injection and downward in the case of suction. It is also noted that the transverse velocity is relatively large near the inlet, but small in the fully developed region of the duct flow. In particular, most of the z-direction velocity components can be neglected if the flow is fully developed hydrodynamically. These results further support the conventional assumptions of transverse velocities, v and w, used by Berman in a parallel-plate flow with porous walls [19] and by Yuan and Finkelstein in a porous pipe flow [20].

Pressure variation

The axial pressure along the axial direction is illustrated in Fig. 6 for various wall Reynolds numbers. For an impermeable flow $Re_w = 0$, axial pressure continuously decreases in the developing region. A fixed value of the pressure gradient is obtained when the flow reaches its fully developed region. For injection flow, the axial pressure decreases faster for larger Re_w. This additional pressure drop is necessary for overcoming the flow resistance induced by the injection fluid flow.

Figure 6 also shows the dimensionless pressure pro-

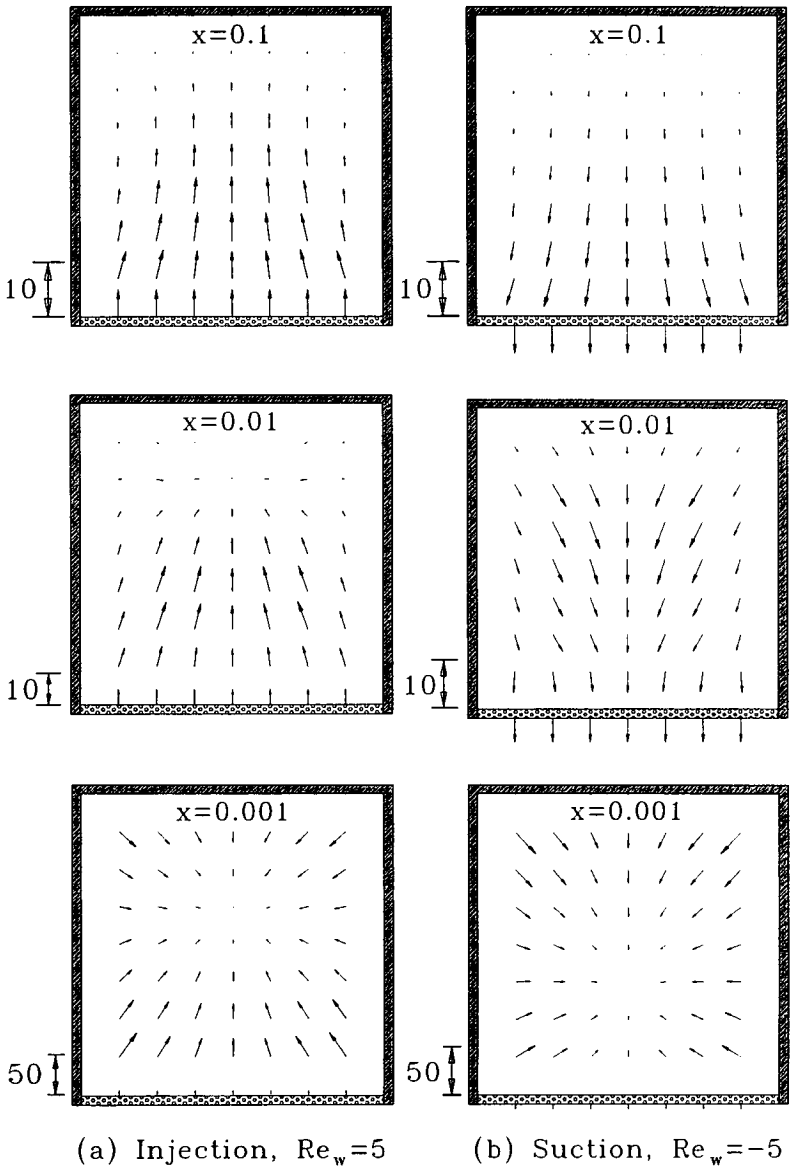

FIG. 5. Vector plots of transverse velocity distributions at different axial distances: (a) injection, $Re_w = 5$; (b) suction, $Re_w = -5$.

file of suction flow along the duct for a number of wall Reynolds numbers. At weak suction, the pressure decreases along the duct due to viscous force. However, at higher suction pressure tends to arrive at a constant value as the inertia and viscous forces of the flow counterbalance. When the flow reaches the point of flow reversal, pressure recovery can be observed, as also noted by Rhee and Edwards [2]. The location $x = 0.083$ indicates the point of pressure recovery for $Re_w = -11.5$ which is the critical wall Reynolds number below which flow reversal occurs.

From the concept of pressure deviation, the pressure gradient in the dimensionless x-directional momentum equation can be written as

$$-\frac{\partial p}{\partial x} = -\frac{\mathrm{d}\bar{p}}{\mathrm{d}x} - \frac{1}{Re_0^2}\frac{\partial p'}{\partial x}. \tag{21}$$

Invoking the assumption of fast flow at the inlet, $Re_0 \gg 0$, the last term on the right-hand side of equation (21) can be neglected. For suction flow, this condition would also exist before the flow reversal. But in the case of high suction rate, $Re_w = -20$, the positive value of $-\mathrm{d}\bar{p}/\mathrm{d}x$ along the axial distance decreases to zero and then changes to a negative quantity, thus the assumption, $-\mathrm{d}\bar{p}/\mathrm{d}x \gg (1/Re_0^2)(\partial p'/\partial x)$, is not met at or near the inversion point. However, from the results of Rhee and Edwards [2] for laminar entrance flow in

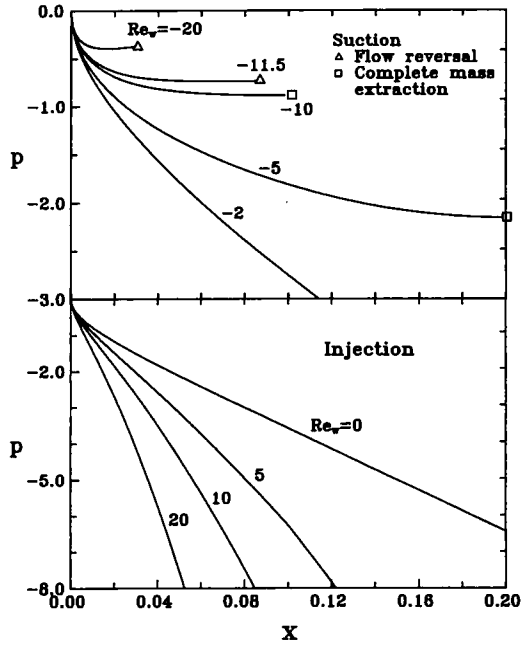

FIG. 6. Wall Reynolds number effects on pressure distributions along the axial direction.

a flat-plate duct with one-walled suction and heating: the pressure drop dominates at lower suction rate, the inertia and viscous effect counterbalance each other at medium suction rate, and pressure recovery is finally observed at higher suction rate. The pressure is nearly constant at the inversion point, both terms on the right-hand side of equation (21) can be neglected. Without the assumption, $-\mathrm{d}\bar{p}/\mathrm{d}x \gg (1/Re_0^2)(\partial p'/\partial x)$, the calculation process can also be proceeded through the inversion point.

Temperature distribution

As mentioned above, only the porous wall located at the bottom of the square duct is heated with a constant heat flux condition. The other three walls are considered adiabatic. Figures 7(a) and (b) show the temperature distributions at axial distances $x^+ = 0.001$, 0.01 and 0.1 for $Re_w = 5$ and -5, respectively. Here, the coordinate for thermal plots in the thermal entrance region is normalized to $x^+ = x/Pr$ in order to compare with data in the open literature. Because heat is transferred through the porous wall, the temperature in the lower area is higher. Since the side walls are adiabatic and the center portion of the duct is cooled by the upstream fluid, temperatures close to the two side walls are higher than those in the center. Notice also that the temperature at any position in the cross section for injection flow is always larger than that for suction flow, except in the entrance region where the difference may not be obvious. From the isotherm maps, both magnitudes and variations of the temperatures in each cross section can be clearly observed. This information is helpful for the system design, for example, of a fuel cell stack. In solid oxide fuel cells [21], the operating temperature is normally at 1000°C, thermal cracking is one of the major problems to be overcome.

The effect of Re_w on the temperature profiles is illustrated in Fig. 8 for both injection and suction flows. The thickening of the thermal boundary layer for injection flow is slower than those of suction and impermeable flows. In addition, a larger magnitude of the wall Reynolds number results in slower development of the thermal boundary layer. Figure 8 also shows that the temperature at a fixed axial location is always higher for injection flow than for suction flow due to larger heat input.

For practical applications, the average porous wall temperature and bulk mean temperature of the fluid along the channel are important. As shown in Fig. 9, the average dimensionless temperature of the porous wall is always higher than the bulk mean temperature of the fluid at any axial position due to the heat transferred at the porous wall. The injected fluid with temperature θ_w increases the temperature of the fluid in the duct for injection flow. Consequently, θ_w will be affected by the fluid temperature and becomes larger for higher Re_w. On the contrary, the fluid temperature at a fixed axial location decreases in suction flow, where the wall temperature is reduced and becomes smaller for stronger suction. For a fully developed flow without injection or suction, the variation of bulk mean temperature is linear as indicated by the line labeled with $Re_w = 0$ in Fig. 9. Similarly, the bulk mean temperature at a fixed axial location is increased by the thermal effect of fluid injection, but is reduced by fluid extraction. The trend is more enhanced for larger absolute values of wall Reynolds numbers.

Friction factor

Typical variations of skin friction along the axial direction in a square duct for both injection and suction flow are shown in Fig. 10. In the case of injection flow, friction factors gradually decrease as Re_w increase for $x < 0.002$, but increase as Re_w increases for $x > 0.002$. According to equation (14), the local friction factor is affected by both averaged axial velocity and wall velocity gradient. As noted previously, boundary layers are formed near the four walls close to the inlet, and the fluid is forced into the center portion of the duct. Axial velocity gradients are almost the same for different Re_w here. As a result, friction factors are dominated by the average axial velocity. However, when the flow is further developed along the x-direction, the wall velocity gradient dominates the variation of friction factor. Consequently, increasing wall velocity gradient due to larger wall Reynolds numbers results in higher values of friction factors.

Turning to suction flow, the friction factor increases as suction increases in the region close to the inlet according to the reason explained above. However, at larger x, friction factors become more complicated. From the results of present computations, the friction factor in suction flow can be explained as follows:

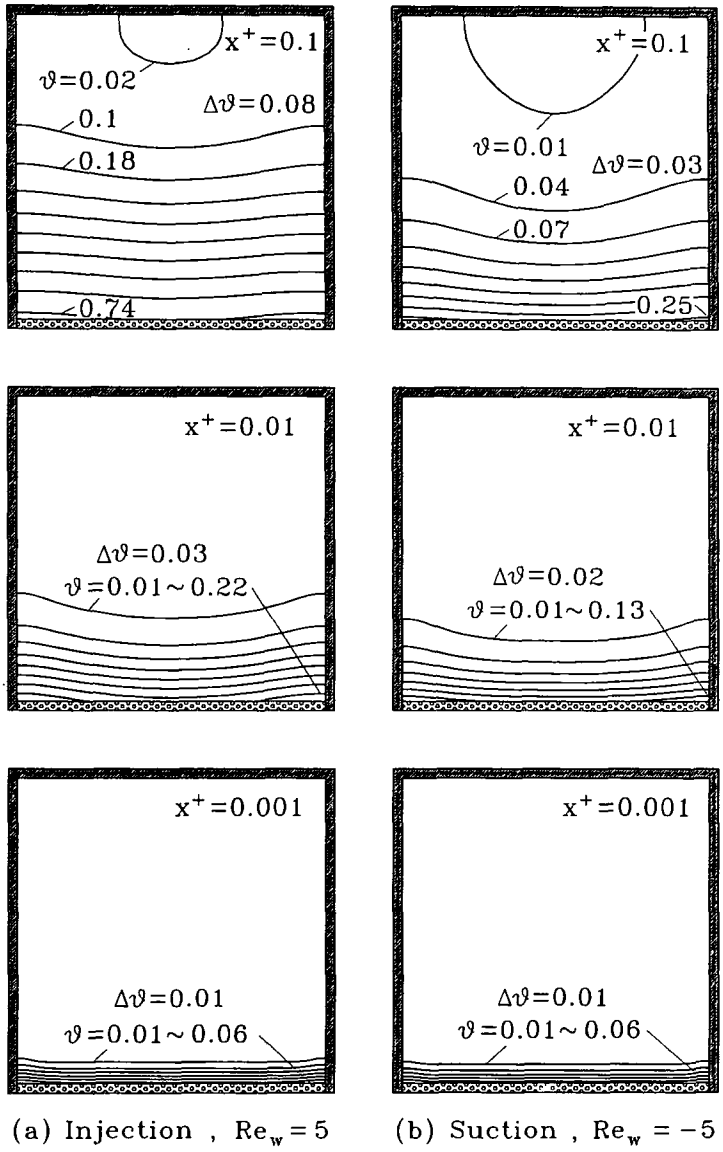

FIG. 7. Isotherm maps at different axial distances: (a) injection, $Re_w = 5$; (b) suction, $Re_w = -5$.

(1) For the case of weak suction flow ($-11.5 < Re_w < 0$), the flow can proceed to the point of complete mass extraction without flow reversal. For instance, at $Re_w = -5$, the friction factor reaches a constant value at large axial distance due to the decreasing velocity gradient similar to injection flow. However, at $Re_w = -10$, the value of $f\,Re$ increases after $x = 0.04$ due to the effect of mass extraction.

(2) For the case of strong suction flow ($Re_w < -11.5$), suction at the wall induces flow reversal at a specific point before the flow reaches complete extraction. Hence, the calculation procedure is terminated at this point. In addition, the minimum friction factors occur at $x = 0.03$ for $Re_w = -11.5$ and at $x = 0.018$ for $Re_w = -20$. These locations are seen moving toward the inlet region as the suction increases.

It is also seen in Fig. 10 that the entrance length is reduced by fluid injection. However, the suction flow cannot reach its fully developed region due to the effects of complete mass extraction or flow reversal.

Heat transfer

The effect of Re_w on Nusselt numbers along the axial direction for $Pr = 0.72$ in the thermal entrance region is given in Fig. 11. As can be seen, heat transfer is reduced by fluid injection and is increased by fluid suction. This is similar to the solutions of Peterson and Kinney [22] for porous tubes and Doughty and Perkins [23] for porous parallel plates. The temperature of the porous heated wall is larger than the bulk mean temperature for all cases. In the case of injection flow, both θ_w and θ_b along the axial direction increase due to heat transfer from the porous wall

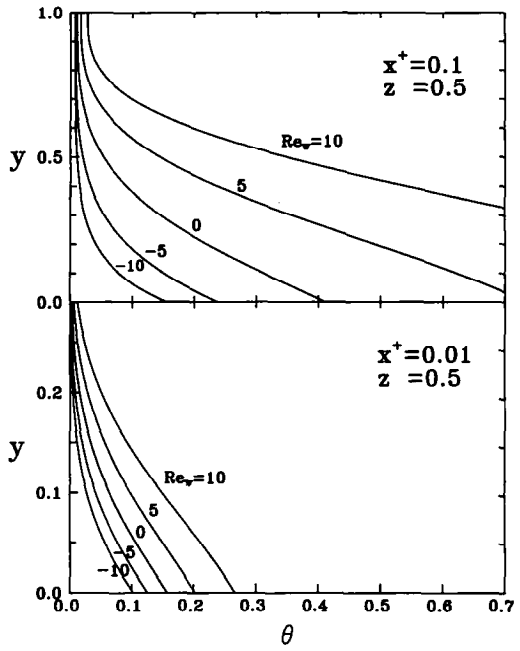

FIG. 8. Wall Reynolds number effects on temperature distributions at different axial distances.

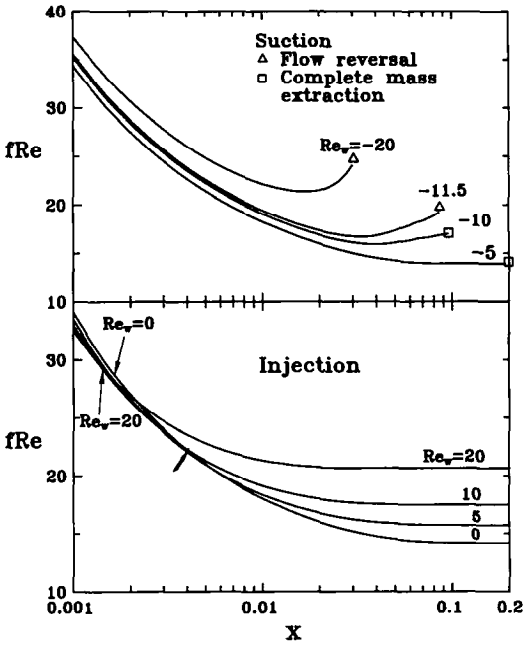

FIG. 10. Wall Reynolds number effects on friction factors along the axial direction.

and the injected fluid along the duct. Their difference gradually approaches a constant value in the fully developed region. In the case of suction flow, the temperature difference of heated wall and bulk fluid is reduced by fluid extraction, and hence the Nusselt number is larger than that of injection flow at the same axial position.

The effect of Prandtl number on heat transfer of a duct flow with fluid injection or suction along the axial direction is illustrated in Fig. 12. It is seen in this figure that the Nusselt number is strongly affected by the fluid Prandtl number. Understandably, heat injected into or extracted from the main stream depends on the fluid heat capacity. At large Prandtl number, the transverse convective heat transport is larger than the axial convective heat transfer. As a result, increasing Prandtl number decreases Nusselt number in the case of injection flow at fixed Re_w while the result is reversed in the case of suction flow. Furthermore, it can be obtained readily from equation (17) that, away from the inlet, heat transfer for suction flow can be expressed by

$$Nu = -Re_w Pr. \tag{22}$$

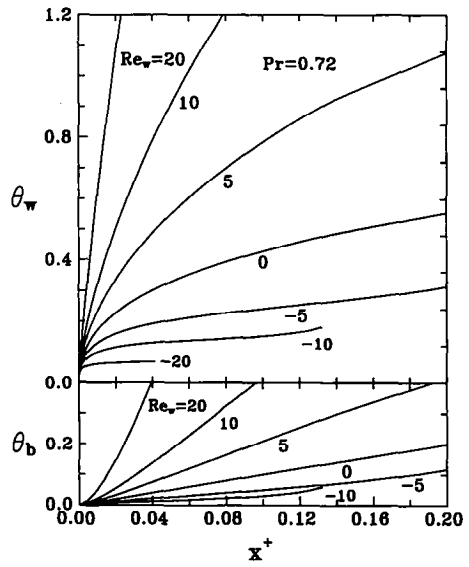

FIG. 9. Wall Reynolds number effects on porous wall and bulk mean temperature distributions along axial direction.

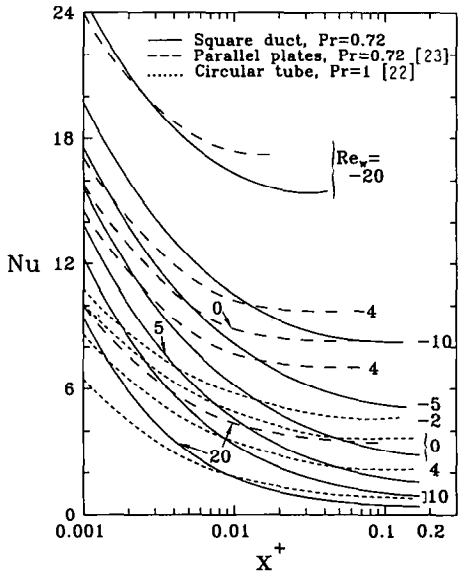

FIG. 11. Wall Reynolds number effects on Nusselt numbers along the axial direction.

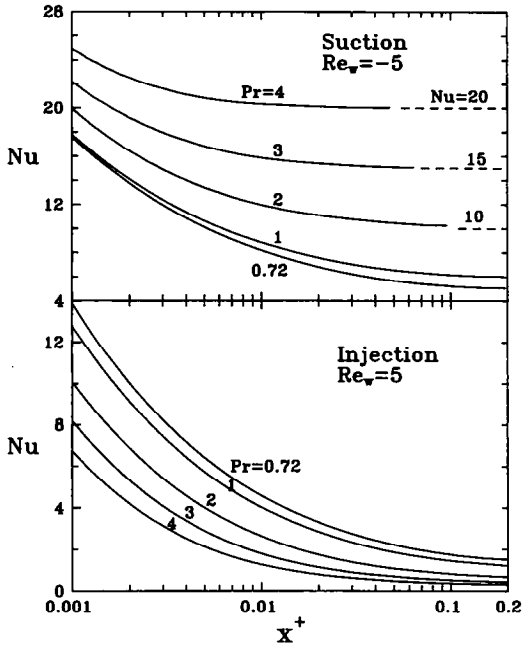

FIG. 12. Prandtl number effects on Nusselt numbers along the axial direction.

This is illustrated graphically in Fig. 12, in which Nusselt numbers for $Pr = 2, 3$ and 4 approach asymptotic values given by equation (22). Similar results have been reported by Kinney [24] in porous tube flows.

Correlations for fully developed data

Fully developed friction factors for injection flow are presented in Table 3. This table does not include the cases of suction flow in which the hydrodynamically and thermally developed regions do not exist. The friction factors for the injection flow in the fully developed region can be correlated within 1% for $Re_w < 20$ by

$$f\,Re_{fd} = 14.23 + 0.322\,Re_w, \quad 0 < Re_w < 20 \quad (23)$$

where 14.23 is the value of $f\,Re$ for impermeable square duct flows [15].

Table 3 also presents fully developed Nusselt numbers for different rates of fluid injection. For large injection, Nu is very small; hence the thermal energy input to the flow is mainly from the injected fluid. A similar correlation for fully developed Nusselt numbers for injection flow can be expressed as

$$Nu_{fd} = 2.712 - 0.367\,Re_w + 0.0212\,Re_w^2 - 0.000443\,Re_w^3, \quad 0 < Re_w < 20 \quad (24)$$

where 2.712 is the value of Nu for impermeable square duct flows [17]. Equation (24) is correlated within 4% for $Re_w < 20$ at $Pr = 0.72$.

CONCLUSIONS

The following statements can be made:

(1) The axial pressure drop in a square channel is reduced for injection flow and is increased for suction flow as compared with impermeable flow. However, the pressure recovery appears downstream for $Re_w < -11.5$ due to flow reversal, and the laminar flow may then change to turbulent flow.

(2) It is shown that fluid injection increases friction factors and reduces the entrance length. However, a fully developed region is not achieved eventually for suction flow due to mass extraction and flow reversal.

(3) For a given Prandtl number, it has been verified that the wall heat transfer decreases in injection flow and increases in suction flow. Similarly, at fixed Re_w, increasing Prandtl number decreases Nusselt number for injection flow and increases Nusselt number for suction flow. For the case of suction flow at Prandtl number higher than 2, the Nusselt number reaches a limit of $-Re_w\,Pr$ away from the inlet.

(4) New correlations on friction factors and heat transfer of fully developed injection flow are proposed in the present study. These correlations can be reduced to impermeable flow as $Re_w = 0$.

Acknowledgements—This study is supported by the Energy Commission of the Ministry of Economic Affairs of the Republic of China through its fuel cell project No. 33K6000-J1. The authors also acknowledge the assistance of the Energy and Resources Laboratories, ITRI for the use of their computer.

REFERENCES

1. G. D. Raithby and D. C. Knudsen, Hydrodynamic development in a duct with suction and blowing, *J. Appl. Mech.* **41**, 896–902 (1974).
2. S. J. Rhee and D. K. Edwards, Laminar entrance flow in a flat plate duct with asymmetric suction and heating, *Numer. Heat Transfer* **4**, 85–100 (1981).
3. C. Y. Soong and G. J. Hwang, Laminar mixed convection in a radially rotating semiporous channel, *Int. J. Heat Mass Transfer* **33**, 1805–1816 (1990).
4. P. L. Donoughe, Analysis of laminar incompressible flow in semiporous channels, TN-3759, NACA (1956).
5. E. R. G. Eckert, P. L. Donoughe and B. J. Moore, Velocity and friction characteristics of laminar viscous boundary-layer and channel flow over surfaces with ejection and suction, TN-4102, NACA (1957).
6. M. M. Sorour and M. A. Hassab, Effect of sucking the hot fluid film on the performance of flat plate solar energy collectors, *Appl. Energy* **14**, 161–173 (1983).
7. P. Lessner and J. Newman, Hydrodynamics and mass transfer in a porous-wall channel, *J. Electrochem. Soc.* **131**, 1828–1831 (1984).
8. M. M. Sorour, M. A. Hassab and S. Estafanous, Developing laminar flow in a semiporous two-dimensional channel with nonuniform transpiration, *Int. J. Heat Fluid Flow* **10**, 44–54 (1987).
9. A. J. Appleby and F. R. Foulkes, *Fuel Cell Handbook*, pp. 503–510. Van Nostrand Reinhold, New York (1989).
10. D. Gidaspow and B. S. Baker, Heat transfer in a fuel cell battery, *A.I.Ch.E. Jl* **11**, 825–831 (1965).
11. F. C. Chou and G. J. Hwang, Vorticity–velocity method for the Graetz problem and the effect of natural con-

vection in a horizontal rectangular channel with uniform wall heat flux, *J. Heat Transfer* **109,** 704–710 (1987).
12. T. C. Jen, A. S. Lavine and G. J. Hwang, Simultaneously developing laminar convection in rotating isothermal square channels, *Int. J. Heat Mass Transfer* **35,** 239–254 (1992).
13. P. J. Roache, *Computational Fluid Dynamics*, pp. 61–64. Reinhold, New York (1971).
14. D. A. Anderson, J. C. Tannchill and R. H. Pletcher, *Computational Fluid Mechanics and Heat Transfer*, pp. 136–137. Hemisphere, Washington, DC (1984).
15. R. A. Shah and A. L. London, *Laminar Flow Forced Convection in Ducts, Suppl. 1 to Adv. Heat Transfer*, pp. 196–222. Academic Press, New York (1978).
16. R. M. Curr, D. Sharma and D. G. Tatchell, Numerical prediction of some three-dimensional boundary layers in ducts, *Comput. Meth. Appl. Mech. Engng* **1,** 143–158 (1972).
17. F. W. Schmidt and M. E. Newell, Heat transfer in fully developed laminar flow through rectangular and isosceles triangular ducts, *Int. J. Heat Mass Transfer* **10,** 1121–1128 (1967).
18. J. P. Quaile and E. K. Levy, Laminar flow in a porous tube with suction, *J. Heat Transfer* **97,** 66–71 (1975).
19. A. S. Berman, Laminar flow in channels with porous walls, *J. Appl. Phys.* **24,** 1232–1235 (1953).
20. S. W. Yuan and A. B. Finkelstein, An incompressible pipe flow with injection and suction through a porous wall, *ASME Trans.* **88,** 719–724 (1956).
21. K. Kinoshita, F. R. McLarnon and E. J. Cairns, *Fuel Cell—A Handbook*, METC-88/6096. DOE (1988).
22. R. J. Pederson and R. B. Kinney, Entrance-region heat transfer for laminar flow in porous tubes, *Int. J. Heat Mass Transfer* **14,** 159–161 (1971).
23. J. R. Doughty and H. C. Perkins, Jr., Thermal and combined entry problems for laminar flow between parallel porous plates, *J. Heat Transfer* **94,** 233–234 (1972).
24. R. B. Kinney, Fully developed frictional and heat transfer characteristics of laminar flow in porous tubes, *Int. J. Heat Mass Transfer* **11,** 1393–1401 (1968).